Diagn Interv Radiol 2019; 25:291–297

INTERVENTIONAL RADIOLOGY

ORIGINAL ARTICLE

Subsequent cooling-circulation after radiofrequency and microwave ablation avoids secondary indirect damage induced by residual thermal energy

Xinyi Shi*
Hong Pan*
Han Ge*
Li Li
Yi Xu
Cong Wang
Hui Xie
Xiaoan Liu
Wenbin Zhou
Shui Wang

PURPOSE
We aimed to investigate the exact role of residual thermal energy following microwave ablation (MWA) and radiofrequency ablation (RFA) at the final ablation and transition zones and determine whether residual thermal energy could be dissipated by subsequent cooling-circulation.

METHODS
In an *ex vivo* study, MWA and RFA were performed on fresh porcine liver, and central and border temperatures were compared. In an *in vivo* study, MWA and RFA were performed to the livers of New Zealand white rabbits. Tissue samples were stained with α-NADH-diaphorase. The coagulation zones (NADH-negative) and transition zones (lightly NADH-stained) of different groups were compared at different time points.

RESULTS
In the *ex vivo* model, the residual thermal energy after MWA and RFA could be dispersed by subsequent cooling-circulation due to the temperature decreasing rapidly. In the *in vivo* study, the coagulation volume in the ablation group was larger than that in the cooling-circulation group ($P < 0.05$) 2 days after ablation. In the ablation group, the damaged zone (the transition zone plus the coagulation zone) on α-NADH-diaphorase-stained images increased rapidly within 2 hours after ablation and slowly reached the maximum on day 2. However, the damaged zones did not change significantly at the three time points observed in the cooling-circulation group.

CONCLUSION
The residual thermal energy in MWA and RFA induced secondary damage beyond the direct coagulation zone, and it could be dissipated by subsequent cooling-circulation, contributing to smaller ablation and transition zones.

Radiofrequency ablation (RFA) and microwave ablation (MWA) have been widely used clinically in the treatment of liver tumors and some other solid tumors (1–4). RFA and MWA destroy tumors *in situ* through thermal coagulation or protein denaturation. RFA creates ionic agitation, which produces frictional heat and heat conduction to achieve subsequent tissue necrosis (5, 6). MWA applies electromagnetic energy to rotate adjacent polar water molecules rapidly (7). Previous studies (2–4, 8) have demonstrated that both MWA and RFA are safe, minimally invasive therapeutic options for solid tumors.

However, traditional non-cooled probes are subject to high-power feedback, so the shaft temperature becomes high, contributing to limitations for thermal therapies (7, 9–11). Temperatures near the electrode or antenna range between 60°C and 100°C, and this results in an area of instant coagulation necrosis (12, 13). The thermal energy disperses to the peripheral area around the coagulation necrosis area and causes secondary damage to ablation zone, resulting in a prolonged damaged zone after ablation (6, 14). Interestingly, the coagulation volumes induced by RFA *in vivo* reach the maximum on day 2 (15). In our present study, the residual thermal energy was defined as the thermal energy released from the ablation area when the temperature after ablation gradually decreases to the body temperature. It seems that residual thermal energy may play an important role in enlarging the ablation zone volume.

From the Departments of Breast Surgery (X.S., H.P., H.G., L.L., H.X., X.L., W.Z., ✉ *zhouwenbin@njmu.edu.cn*, S.W. ✉ *ws0801@hotmail.com*) and Pathology (Y.X., C.W.), The First Affiliated Hospital of Nanjing Medical University, Nanjing, China.

* These authors contributed equally to this work.

Received 12 January 2018; revision requested 10 February 2018; last revision received 21 August 2018; accepted 10 September 2018.

Published online 14 May 2019.

DOI 10.5152/dir.2019.17455

You may cite this article as: Shi X, Pan H, Ge H, et al. Subsequent cooling-circulation after radiofrequency and microwave ablation avoids secondary indirect damage induced by residual thermal energy. Diagn Interv Radiol 2019; 25:291–297.

Table. The groups and the volume of ablation zone in the *ex vivo* study

	MWA		RFA	
Ablation volumes	Ablation alone	Subsequent cooling-circulation	Ablation alone	Subsequent cooling-circulation
From 0 to 2 cm^3	10 W, 15 min	10 W, 15 min	10 W, 15 min	10 W, 15 min
	20 W, 7 min	20 W, 7 min	15 W, 10 min	15 W, 10 min
	15 W, 10 min	15 W, 10 min	20 W, 5 min	20 W, 5 min
From 2 to 4 cm^3	40 W, 5 min	40 W, 5 min	15 W, 15 min	15 W, 15 min
	20 W, 10 min	20 W, 10 min	15 W, 20 min	15 W, 20 min
	60 W, 5 min	60 W, 5 min	20 W, 10 min	20 W, 10 min
From 4 to 6 cm^3	10 W, 30 min	10 W, 30 min	15 W, 30 min	15 W, 30 min
	40 W, 10 min	40 W, 10 min	20 W, 15 min	20 W, 15 min
	60 W, 7 min	60 W, 7 min	20 W, 20 min	20 W, 20 min

MWA, microwave ablation; RFA, radiofrequency ablation.

Currently, internally cooled probes are applied in MWA and RFA (8, 16–18). Cooled electrodes and cooling systems can reduce the temperature at the electrode tissue interface, avoid skin injury (19), and attain larger necrosis volumes (14). Therefore, it is assumed that subsequent cooling-circulation after ablation may effectively reduce the tissue temperature after ablation. However, whether the residual thermal energy could be effectively dissipated by a cooling system is not known. In this study, we kept the needle in the liver with the ablation function turned off and retained the water-cooling function for 10 min after ablation. We reasoned that the residual thermal energy can be dissipated by subsequent cooling-circulation after ablation.

The purpose of this study was to determine the exact role of residual thermal energy in MWA and RFA on the final ablation zone and transition zone and investigate whether the additional damaged zone caused by the residual thermal energy could be dissipated by subsequent cooling-circulation after ablation.

Main points

- The residual thermal energy after MWA and RFA could be dispersed by subsequent cooling-circulation.
- The cooling-circulation after MWA and RFA decreased the coagulation volume.
- The subsequent cooling-circulation of MWA and RFA could control the ablation range by adjusting residual thermal energy.

Methods

Microwave and radiofrequency systems

The microwave unit (ECO-100E, Eco Medical) consisted of a microwave generator, a flexible coaxial cable, a water-pumping machine and a needle antenna with two lumens in the shaft to circulate the cooling water (8). The microwave irradiation frequency was 2450 MHz. The output powers could be modulated from 10 to 100 W. The 2 mm long irradiating segment was embedded in the front of the needle antenna and 11 mm away from the shaft tip. The socket at the end of the needle antenna was used to connect the plug of the cable coming from the microwave generator.

All of the RFA procedures in this study were performed with a 480 KHz radiofrequency generator (S-5L, MedSphere International) that provided a maximum power output of 50 W. Radiofrequency energy was deposited by using an internally cooled applicator with a cool-tip single-needle electrode. When the generator is operated in automatically pulsed mode according to the manufacturer's recommendations during ablation, the output is controlled by an algorithm with an impedance feedback loop that is used to maximize energy delivery by minimizing charring. The electrode shaft was a 16-gauge monopolar electrode with two lumens that enabled internal fluid circulation and active stainless steel tip exposure of 2 cm.

Ex vivo study protocol

Fresh porcine liver blocks were obtained from a slaughterhouse. The liver blocks were immersed in a thermostat water bath under incubation at 37°C and filled with normal saline. The cooling water bottle was submerged in ice to maintain the temperature of the circulating water at 0°C. The microwave antenna and radiofrequency electrode were inserted at least 7 cm into the liver to ensure that the entire ablation zone would be within the liver parenchyma.

In this study, the central temperature and border temperature (the temperature of the coagulation zone borderline) were compared between the ablation group and the subsequent cooling-circulation group. The ablation group in this study refers to ablation of the liver with the ablation function and water-cooling function turned on and the water-cooling function turned off immediately after ablation under the below-mentioned power and time. Subsequent cooling-circulation refers to keeping the needle in the liver after the ablation function turned off but retaining the water-cooling function for 10 min (moderate duration). In our preliminary experiment, the ablation volumes of porcine livers were evaluated in *ex vivo* study with different power and time combinations. According to the ablation volumes, 9 power and time combinations were applied for both MWA and RFA in this study (Table). Each power and time setting were applied for 6 ablations (ablation alone for 3 and sequential cooling for 3), and a total of 108 ablations were performed (Table). All microwave and radiofrequency devices were placed with ultrasound guidance, with the shafts 2 cm or farther away from the large hepatic

vessels visible on grey-scale ultrasound in three planes. The active element of each device was fully embedded in the hepatic parenchyma, with the proximal edge at least 1 cm deep into the liver capsule. Two ablations were applied to each whole lobe of liver (MWA/RFA and subsequent cooling-circulation), which were sufficiently far from each other to prevent collateral heating. The distance between the two ablation centers was more than 5 cm.

After ablation or sequential cooling-circulation, the liver blocks were dissected along the probe remaining in the lesions and shot by an infrared thermographer (testo890-1, Testo AG) at once. An infrared thermal imaging system was used to transform the infrared energy into visible heat images. The different colors of the temperature distribution graphs represented the different temperatures of the object being measured.

The long diameter (Dl, along the needle insertion axis) and short diameter (Ds, perpendicular to the longitudinal plane) of the coagulation zone were assessed macroscopically with calipers. The diameters were measured from the coagulation zone (the center of the charring zone and white coagulation zone), not from the surrounding red congestion zone of partial necrosis. According to previous studies (20, 21), the coagulation zone was considered an ellipsoid. The volume of necrosis was calculated using the following formula:

$$V = \frac{4\pi}{3}\frac{Dl}{2}\left(\frac{Ds}{2}\right)^2$$

In vivo study protocol

The study was approved by the Institutional Animal Care and Use Committee. All applicable institutional and national guidelines for the care and use of animals were followed. Male New Zealand white rabbits (age range, 12–14 weeks; weight range, 2.0–2.5 kg) were used. Anesthesia was induced through an intravenous injection of pentobarbital (30 mg/mL, 0.8–1.2 mL/kg, pentobarbital sodium; Sigma). Bilateral subcostal incisions were applied to expose the liver. Four groups of different ablations were performed to the liver of each New Zealand white rabbit: MWA (MWA with the ablation function and water-cooling function turned on and the water-cooling function turned off immediately after ablation under 20 W for 7 min), MWA cooling (subsequent cooling-circulation for 10 minutes after MWA under 20 W for 7 min), RFA (RFA with the ablation function and water-cooling function turned on and the water-cooling function turned off immediately after ablation after RFA under 20 W for 5 min) and RFA cooling (subsequent cooling-circulation for 10 minutes after RFA under 20 W for 5 min). According to our *ex vivo* study, 20 W 7 min of MWA and 20 W 5 min of RFA were selected because that they were closest volumes obtained in the *ex vivo* study, which were also suitable for 4 ablations to one whole rabbit liver. One ablation was applied to the right lobe, and the other three ablations were applied to the left lobes (2 to the larger left lobe and 1 to the other left lobe). Proper placement of the ablation needle was guided by ultrasound to avoid vessels with diameters larger than 5 mm. The distance between the two ablation centers was more than 5 cm. The needle was 1.5 cm from the surface of the liver. After all of the ablations were finished, the rabbits were sacrificed at 0 hour, 2 hours and 48 hours, and the entire livers were harvested immediately after sacrifice. A total of 24 ablations (6 ablations per group) in 6 rabbits were performed at each time point. A total of 72 ablations were performed in all.

Each ablated zone was dissected along the axis of the probe insertions. The ablated zones were sectioned along the antenna shaft. The sections were stained with α-nicotinamide adenine dinucleotide, reduced-diaphorase (α-NADH-diaphorase), and the long diameters and short diameters were assessed by the stained sections.

Pathologic examination

In the *in vivo* study, the ablated tissue was harvested at three time points. Samples were frozen in liquid nitrogen. Cryosections of 8 μm thick slices were placed on glass slides and incubated for 20 min at room temperature. The incubation medium consisted of 6.8 mL of α-NADH-diaphorase (Sigma-Aldrich) 1.5 mg/mL, 12.0 mL of nitroblue tetrazolium chloride (Sigma-Aldrich) 2.0 mg/mL, 4.8 mL of phosphate-buffered saline, and 3.8 mL of Ringer solution. The pH of the medium was adjusted to 7.2 before the sections were incubated. After incubation, each slide was washed in distilled water for 2 min. The results of α-NADH-diaphorase staining were evaluated by two pathologists.

Statistical analysis

Numerical data are reported as median (min–max). Differences between groups were analyzed using Kruskal-Wallis test followed by Dunn-Bonferroni post hoc method or a Mann-Whitney U test, when appropriate. All statistical analyses were performed using SPSS 20.0 (IBM Corp.) and $P < 0.05$ was considered to indicate statistically significant differences.

Results

In the *ex vivo* study, the porcine livers were removed and dissected immediately after ablation. Using TestoIRSoft, we found that the center of the coagulation zone showed the highest temperature after ablation and the lowest temperature after cooling-circulation (Fig. 1). The highest temperature after MWA ranged from 64.6°C to 94.6°C. After subsequent cooling-circulation for 10 min, the central temperature dropped to 24.1°C–31.2°C. For RFA, the temperature of the center of the coagulation zone decreased from 57.6°C–82.9°C after ablation to 22.5°C–36.6°C after cooling-circulation.

The temperature distribution profile decreased elliptically from the center to the periphery after both MWA and RFA, and the temperature curve along the long diameter was similar to a downward parabola (Fig. 1). The temperature of the coagulation zone borderline after WMA was 55.7°C–65.7°C. After subsequent cooling-circulation, the temperature distribution elliptically increased from the center to the periphery, and the temperature curve along the long diameter was similar to an upward parabola (Fig. 1). After subsequent cooling-circulation, the temperature of the coagulation zone borderline after MWA was 27.9°C–36.4°C. For RFA, the temperature of the coagulation zone borderline decreased from 45.9°C–65.9°C to 28.6°C–38.7°C.

In each group, the central temperature changed the most among different areas. It decreased from the highest in the coagulation zone to the lowest after subsequent cooling-circulation (Fig. 1). At the same time, the temperature of the coagulation zone borderline also decreased after subsequent cooling-circulation. Almost all of the central and border temperatures after subsequent cooling-circulation decreased quickly and were lower than the temperatures of the tissues and organs (37°C). There was no excess heat conducted to the surrounding tissues. It is supposed, based on these results, that subsequent cooling-circulation after MWA and RFA could dissipate almost all of the residual thermal energy.

In the *in vivo* part of the study, MWA (20

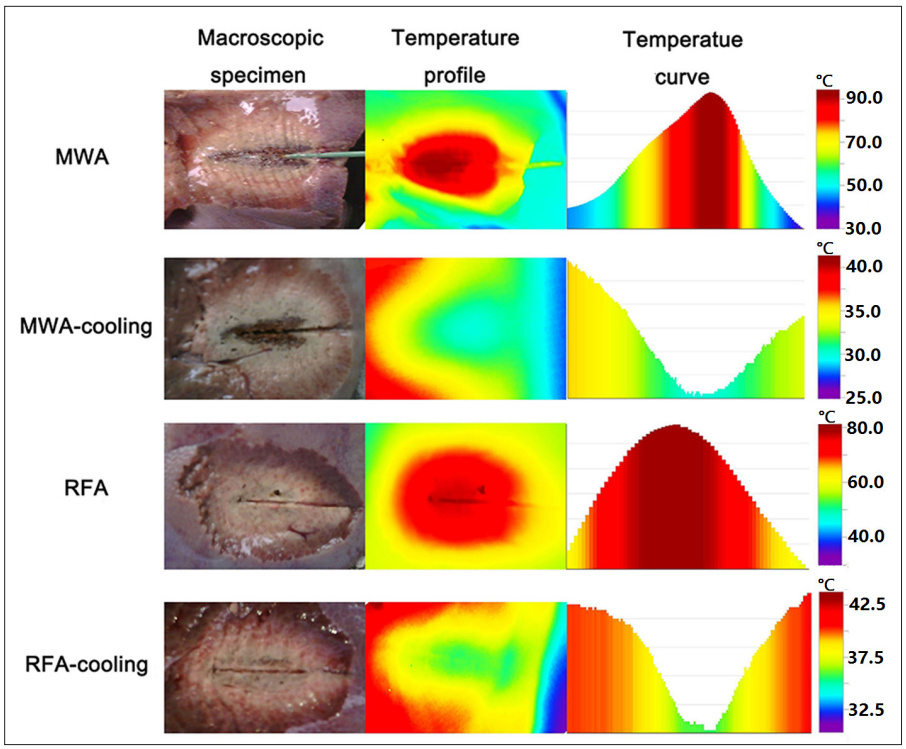

Figure 1. The macroscopic specimens, temperature profiles and temperature curves along the long diameter after MWA (60 W, 7 min), MWA cooling (60 W, 7 min), RFA (20 W, 20 min), and RFA cooling (20 W, 20 min). The temperature distribution profile decreased elliptically from the center to the periphery after both MWA and RFA. After subsequent cooling-circulation, the temperature distribution increased elliptically from the center to the periphery. The center of the coagulation zone showed the highest temperature after ablation and the lowest temperature after cooling-circulation.

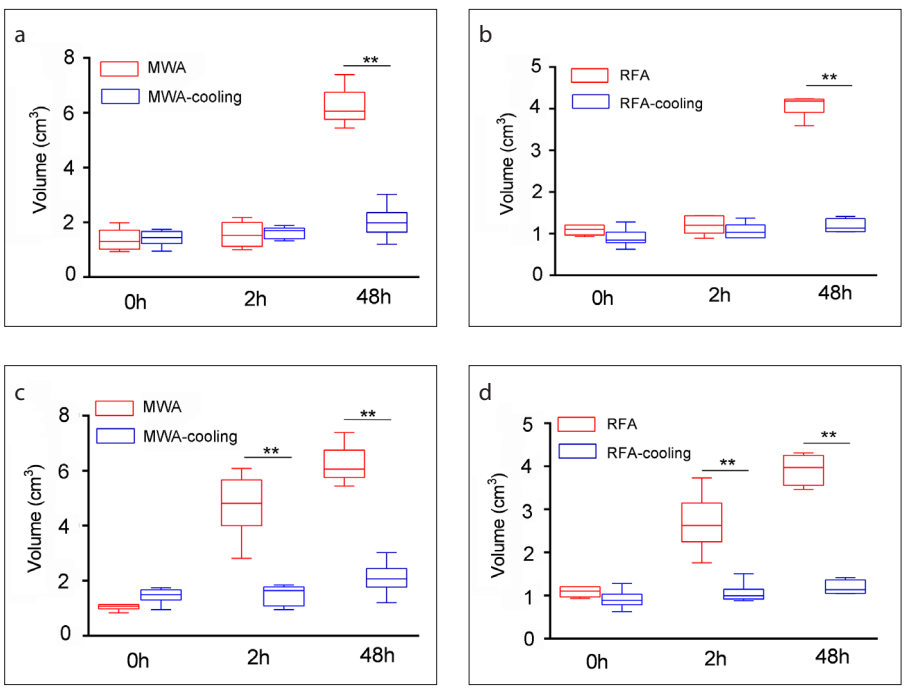

Figure 2. a–d. Graph shows the volumes of the coagulation zone and damaged zone in the MWA, MWA-cooling, RFA, and RFA-cooling groups. At 0 hours and 2 hours after ablation **(a)**, the volumes of the coagulation zone in the MWA group and MWA-cooling group were not significantly different. At 48 hours, the coagulation volume in the MWA group was larger than that in the MWA-cooling group. In RFA **(b)**, similar results for coagulation zone were observed. At 0 hours after ablation **(c)**, the volumes of the damage zone in the MWA group and MWA-cooling group were not significantly different. At 2 hours and 48 hours, the damage volume in the MWA group was larger than that in the MWA-cooling group. In RFA **(d)**, similar results for damage zone were observed (** = $P < 0.001$).

W, 7 min) and RFA (20 W, 5 min) were performed to the livers of New Zealand white rabbits, and four groups of different ablations were applied: MWA, MWA cooling, RFA, and RFA cooling.

There was no significant difference between the long or short diameters of the coagulation zones in the MWA group and the MWA-cooling group at 0 hours and at 2 hours after ablation (long diameters: 0 h, $P = 0.298$, 2 h: $P = 0.364$; short diameters: 0 h, $P = 0.523$, 2 h: $P = 0.697$); however, the long and short diameters of the coagulation zone in the MWA group were significantly longer than those in the MWA-cooling group at 48 hours after ablation (long diameters: $P = 0.002$; short diameters: $P = 0.016$). The volumes of the coagulation zone in MWA and MWA-cooling group had no difference at 0 hours after ablation ($P = 0.699$, Fig. 2a), which represented the damage induced by direct heating. At 2 hours, the volumes of the MWA and MWA-cooling groups were not significantly different ($P = 0.937$, Fig. 2a). However, at 48 hours, the coagulation volume in the MWA group was larger than that in the MWA-cooling group ($P = 0.002$, Fig. 2a). In MWA group, the coagulation zone at 48 hours was larger than that in 0 and 2 hours ($P = 0.004$, $P = 0.024$) (supplemental Table 1). However, in the MWA-cooling group, coagulation zone showed no significant change between 48 hours and 2 hours ($P = 0.479$) (supplemental Table 1).

Similar results were observed for RFA (Fig. 2b). The coagulation zone of RFA and RFA-cooling had no difference at 0 hours ($P = 0.093$, Fig. 2b). At 2 hours, the volumes of the RFA and RFA-cooling groups were not significantly different ($P = 0.309$, Fig. 2b). However, at 48 hours, the coagulation volume in the RFA group was larger than that in the RFA-cooling group ($P = 0.002$, Fig. 2b). In the RFA group, the coagulation zone at 48 hours was larger than that in 0 and 2 hours ($P = 0.004$, $P = 0.026$, respectively) (supplemental Table 2). In the RFA-cooling group, no significant change was observed between the coagulation zones at 48 hours and 2 hours ($P = 0.479$) (supplemental Table 2).

The damage zone in MWA was larger than that in MWA-cooling at 2 hours and 48 hours ($P = 0.002$, $P = 0.002$, respectively) (Fig. 2c). The damage zone at 2 hours and 48 hours in RFA was larger than that in RFA-cooling group (Fig. 2d). The damage zone at 48 hours in the ablation alone or ablation cooling groups was larger than

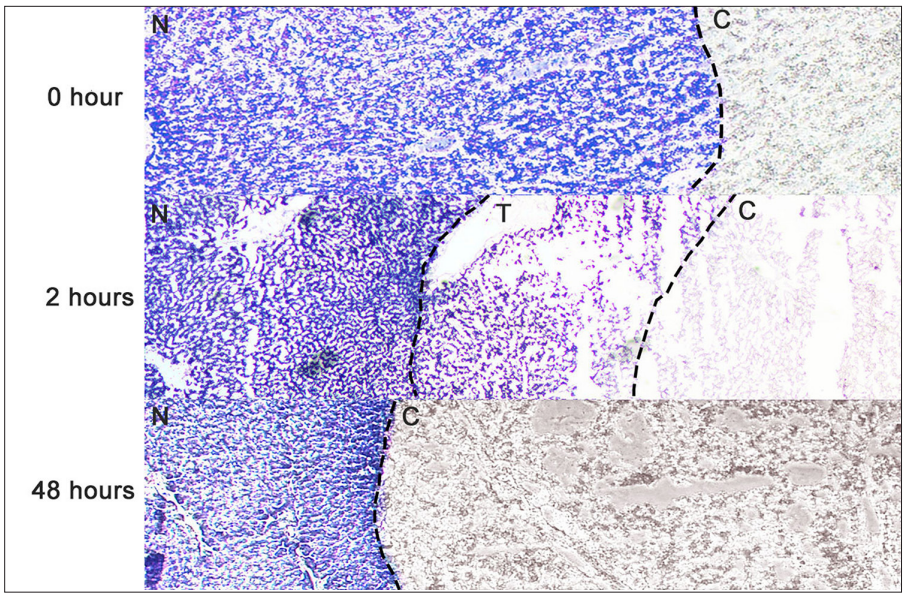

Figure 3. α-NADH-diaphorase-stained image (MWA cooling: 20 W, 7 min) in a representative ablated liver sample shows the typical three zones of tissue change after MWA cooling (20 W, 7 min) at 0 hours, at 2 hours and at 48 hours. The coagulation zone was stained negative, the normal liver was stained dark blue, and the transition zone was stained light blue. Only two zones (the coagulation zone and normal liver zone) were observed at 0 hours and 48 hours after ablation. The transition zone could only be seen at 2 hours (original magnification, ×10; N, the normal liver; C, the coagulation zone; T, the transition zone).

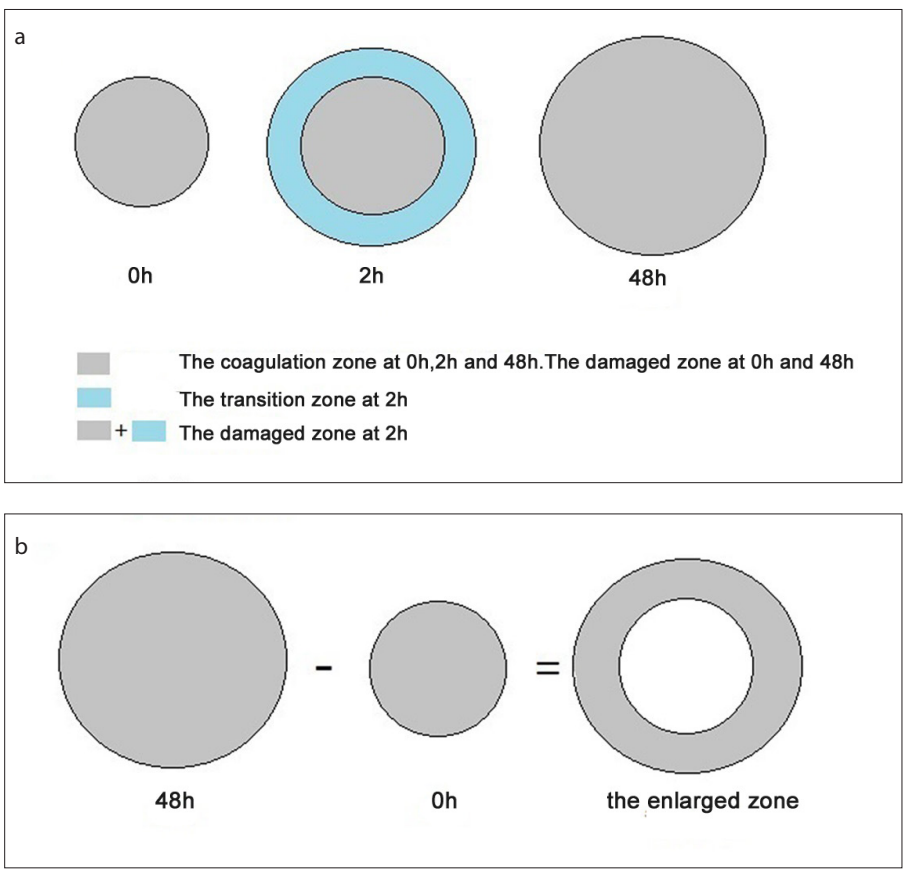

Figure 4. a, b. Definitions of ablation zone patterns. At 0 hours and 48 hours **(a)**, the "damaged zone" was defined as the "coagulation zone". At 2 hours, the "damaged zone" was defined as the "coagulation zone" plus "transition zone", because the transition zone represents part of cell damage, enzyme activity, and completely transformed into "coagulation zone" in 48 hours. The "enlarged zone" **(b)** was defined as the volume of "coagulation zone" at 48 hours minus the volume of "coagulation zone" at 0 hours.

that at 0 hours, and there was no significant change to the damage zone at 48 hours in the ablation alone or ablation cooling groups compared with 2 hours (supplemental Tables 3, 4).

These results suggest that smaller coagulation zones could be obtained when the residual thermal energy is dissipated by cooling-circulation after ablation *in vivo*.

According to the features of α-NADH-diaphorase staining, the negative-stained zone represented the coagulation zone without any viable cells, the dark blue-stained zone represented the normal liver without any dead cells, and the light blue-stained zone represented the transition zone, indicating that the cells were damaged, and partial enzyme viability was preserved (15). Three typical zones were observed on α-NADH-diaphorase-stained images 2 hours after MWA and RFA, including the negative-stained zone, the dark blue-stained zone, and the light blue-stained zone (transition zone) (Fig. 3). However, only two zones (the negative-stained zone and the dark blue-stained zone) were observed 0 hours and two days after ablation, and no transition zone was observed.

In order to facilitate the expression and calculation of the volumes of ablation zone, we defined different types of ablation zones (Fig. 4). The "damaged zone" represented the region in which all cells were damaged. It was defined as coagulation zone at 0 hours and 48 hours, but coagulation zone plus transition zone at 2 hours since the transition zone represented part of cell damage, enzyme activity, and completely transformed into coagulation zone in 48 hours (Fig. 4a). At the same time, the "enlarged zone" represented the damage caused by residual thermal energy. It was defined as the volume of coagulation zone at 48 hours minus the volume of coagulation zone at 0 hours (Fig. 4b).

The volumes of the transition zone and the enlarged zone in the different groups were compared (Fig. 5) (supplemental Tables 5, 6). The volumes of the transition zone in the ablation group were significantly larger than those in the cooling-circulation group. The enlarged areas in the ablation group were significantly larger than those in the cooling-circulation group. However, the transition zone and the enlarged area in the same group were not significantly different (all $P > 0.05$). All of these results suggested that secondary indirect damage induced by

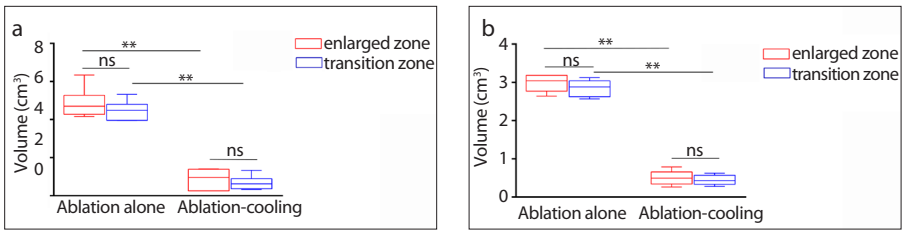

Figure 5. a, b. Comparison of the volumes of the transition zone and the enlarged zone (the volume at 48 hours minus the volume at 0 hours) between the ablation group and the cooling-circulation group. Panel **(a)** shows that the volumes of the transition zone and the enlarged zone in the MWA group were both significantly larger than those in the MWA-cooling group. Panel **(b)** shows that the volumes of the transition zone and the enlarged zone in the RFA group were both significantly larger than those in the RFA-cooling group (** = $P < 0.001$).

residual thermal energy contributed to the formation of the transition zone beyond the direct coagulation zone by MWA and RFA, and secondary indirect damage could be avoided by subsequent cooling circulation after ablation.

Discussion

Previous studies (14, 22) have suggested that direct heat plays an indispensable role in MWA and RFA. In addition, conductive heating of residual thermal energy might also play a role in the process of ablation. However, the type of role that residual thermal energy plays in MWA and RFA is not clear. Our results suggested that the residual thermal energy after MWA and RFA was high. Subsequent cooling circulation after MWA and RFA was able to dissipate all the residual thermal energy from the ablation area. Therefore, residual thermal energy could be avoided by subsequent cooling-circulation after ablation in MWA and RFA.

In our *in vivo* study, a transition zone was seen adjacent to the coagulation zone at 2 hours, and it turned into a negative-stained zone at 2 days. The underlying mechanism of this α-NADH-diaphorase-staining conversion is not clear. A previous study (15) has suggested that the prolonged NADH staining conversion results from slower loss of enzymatic function secondary to microvascular and arteriolar occlusion. However, in the ablation cooling-circulation group, the transition zone was so small that no significant differences among the volumes of the damaged zones at the three different time points were observed. As a result, smaller coagulation zones were obtained when the residual thermal energy was dissipated by cooling-circulation after ablation at 48 hours, suggesting that the residual thermal energy induced secondary indirect damage around the direct heating coagulation zone. Importantly, the temporary transition zone with α-NADH-diaphorase staining 2 hours after ablation was mainly induced by residual thermal energy.

Previous studies (6, 14, 23) have shown that microwave power can be continually applied to produce extremely high temperatures. At the same time, microwave energy has also been shown to ablate tissue up to and around large vessels and seem to create larger zones of ablation in the same high-perfusion areas, whereas radiofrequency energy is limited. In *ex vivo* experiments, the central temperatures after MWA were higher than RFA. After our estimation, the residual thermal energy after MWA was higher than that after RFA. In the *in vivo* study, the enlarged zone in MWA was larger than that in RFA. Thus, the more residual thermal energy remained, the greater the extent of expansion theoretically was. However, further studies will be needed to confirm the inference.

Target tumors can be conceptually divided into three zones: 1) a central area, predominantly treated by thermal ablation, which undergoes heat-induced coagulation necrosis; 2) a peripheral rim, which undergoes reversible changes from sublethal hyperthermia; and 3) the surrounding tumor or normal tissue, which is unaffected by focal ablation (23). For the complete ablation of malignant tumors, the whole tumor should be ablated and a safety margin is required. When the tumor is ablated and a safety margin is obtained based on the immediate assessment after ablation, the ablation should be stopped, but the cooling-circulation system should be kept on to avoid too much damage of normal tissue. When only the ablation of the whole tumor is obtained, both ablation and cooling-circulation system may be stopped since the residual thermal energy can cause further ablation, providing a safety margin. Differently from malignant tumors, only precise ablation of the tumor is required for ideal ablation of benign tumors (24). When the benign tumor is ablated based on the immediate assessment after ablation, the ablation should be stopped and cooling-circulation system should be applied for a while to avoid further damage to normal tissue. In all, two patterns of ablation can be applied: 1) direct heating only; 2) direct heating and conductive heating of residual thermal energy. The right ablation pattern will be chosen based on the ablation zone of the immediate assessment and the tumor type in clinic practice.

Several limitations of this study should be considered. First, although the temperature distribution was obtained immediately after the ablated liver blocks were dissected, part of the thermal energy was still released before the temperature distribution was obtained. Second, the coagulation size in the ablation only group might have been influenced by blood flow *in vivo*; however, the coagulation size in the ablation only group was still significantly larger than that in the cooling-circulation group. Third, normal porcine liver tissue was used during the ablations in our study, rather than tumor tissue. Moreover, thermal energy may affect organs differently, and our results may be organ specific.

In conclusion, the high residual thermal energy in MWA and RFA induced secondary damage beyond the direct coagulation zone, and this energy could be dissipated by subsequent cooling-circulation, contributing to both smaller ablation zone and transition zone. However, the phenomenon was illustrated only in animal experiments in the present study, so further clinical trials are warranted to determine the role of residual thermal energy in MWA and RFA in the treatment of solid tumors.

Financial disclosure

This work was supported in part by the National Natural Science Foundation of China (81572607, 81502299, 81502286 and 81771953), and a project funded by the Priority Academic Program Development of Jiangsu Higher Education Institutions (PAPD).

Conflict of interest disclosure

The authors declared no conflicts of interest.

References

1. Shiomi H, Naka S, Sato K, et al. Thoracoscopy-assisted magnetic resonance guided microwave coagulation therapy for hepatic tumors. Am J Surg 2008; 195:854–860. [CrossRef]

2. Liang P, Dong B, Yu X, et al. Prognostic factors for survival in patients with hepatocellular carcinoma after percutaneous microwave ablation. Radiology 2005; 235:299–307. [CrossRef]
3. Chen MS, Li JQ, Zheng Y, et al. A prospective randomized trial comparing percutaneous local ablative therapy and partial hepatectomy for small hepatocellular carcinoma. Ann Surg 2006; 243:321–328. [CrossRef]
4. Feng K, Yan J, Li X, et al. A randomized controlled trial of radiofrequency ablation and surgical resection in the treatment of small hepatocellular carcinoma. J Hepatol 2012; 57:794–802. [CrossRef]
5. Dos Santos I, Haemmerich D, Schutt D, da Rocha AF, Menezes LR. Probabilistic finite element analysis of radiofrequency liver ablation using the unscented transform. Phys Med Biol 2009; 54:627–640. [CrossRef]
6. Brace CL. Radiofrequency and microwave ablation of the liver, lung, kidney, and bone: what are the differences? Curr Probl Diagn Radiol 2009; 38:135–143. [CrossRef]
7. Yu J, Liang P, Yu X, Liu F, Chen L, Wang Y. A comparison of microwave ablation and bipolar radiofrequency ablation both with an internally cooled probe: results in ex vivo and in vivo porcine livers. Eur J Radiol 2011;79:124–130. [CrossRef]
8. Zhou W, Zha X, Liu X, et al. US-guided percutaneous microwave coagulation of small breast cancers: a clinical study. Radiology 2012; 263:364–373. [CrossRef]
9. Wright AS, Sampson LA, Warner TF, Mahvi DM, Lee FT, Jr. Radiofrequency versus microwave ablation in a hepatic porcine model. Radiology 2005; 236:132–139. [CrossRef]
10. Simon CJ, Dupuy DE, Mayo-Smith WW. Microwave ablation: principles and applications. Radiographics 2005; 25 (Suppl 1):S69–83. [CrossRef]
11. Goldberg SN, Ahmed M, Gazelle GS, et al. Radio-frequency thermal ablation with NaCl solution injection: effect of electrical conductivity on tissue heating and coagulation-phantom and porcine liver study. Radiology 2001; 219:157–165. [CrossRef]
12. Gervais DA, Arellano RS. Percutaneous tumor ablation for hepatocellular carcinoma. AJR Am J Roentgenol 2011; 197:789–794. [CrossRef]
13. Goldberg SN, Gazelle GS, Mueller PR. Thermal ablation therapy for focal malignancy: a unified approach to underlying principles, techniques, and diagnostic imaging guidance. AJR Am J Roentgenol 2000; 174:3233–3231. [CrossRef]
14. Poulou LS, Botsa E, Thanou I, Ziakas PD, Thanos L. Percutaneous microwave ablation vs radiofrequency ablation in the treatment of hepatocellular carcinoma. World J Hepatol 2015; 7:1054–1063. [CrossRef]
15. Wu H, Wilkins LR, Ziats NP, Haaga JR, Exner AA. Real-time monitoring of radiofrequency ablation and postablation assessment: accuracy of contrast-enhanced US in experimental rat liver model. Radiology 2014; 270:107–116. [CrossRef]
16. Miao Y, Ni Y, Yu J, Marchal G. A comparative study on validation of a novel cooled-wet electrode for radiofrequency liver ablation. Invest Radiol 2000; 35:438–444. [CrossRef]
17. Waaijer L, Kreb DL, Fernandez Gallardo MA, et al. Radiofrequency ablation of small breast tumours: evaluation of a novel bipolar cool-tip application. Eur J Surg Oncol 2014; 40:1222–1229. [CrossRef]
18. Wang-Yuan Z, Jiang-Zheng Z, Lu YD, et al. Clinical efficacy of metronomic chemotherapy after cool-tip radiofrequency ablation in the treatment of hepatocellular carcinoma. Int J Hyperthermia 2016; 32:193–198. [CrossRef]
19. Sun Y, Wang Y, Ni X, et al. Comparison of ablation zone between 915- and 2,450-MHz cooled-shaft microwave antenna: results in in vivo porcine livers. AJR Am J Roentgenol 2009; 192:511–514. [CrossRef]
20. Zhou W, Liang M, Pan H, et al. Comparison of ablation zones among different tissues using 2450-MHz cooled-shaft microwave antenna: results in ex vivo porcine models. PLoS One 2013; 8:e71873. [CrossRef]
21. Zhou W, Jiang Y, Chen L, et al. Image and pathological changes after microwave ablation of breast cancer: a pilot study. Eur J Radiol 2014;83:1771–1777. [CrossRef]
22. Przybyla BD, Shafirstein G, Koonce NA, Webber JS, Griffin RJ. Conductive thermal ablation of 4T1 murine breast carcinoma reduces severe hypoxia in surviving tumour. Int J Hyperthermia 2012; 28:156–162. [CrossRef]
23. Ahmed M, Brace CL, Lee FT, Jr., Goldberg SN. Principles of and advances in percutaneous ablation. Radiology 2011; 258:351–369. [CrossRef]
24. Zhou W, Wang R, Liu X, et al. Ultrasound-guided microwave ablation: a promising tool in management of benign breast tumours. Int J Hyperthermia 2016; 33: 1-8. [CrossRef]

Supplemental Table 1. The coagulation zone for MWA and MWA-cooling

	0h (n=6) Median (min-max)	2h (n=6) Median (min-max)	48h (n=6) Median (min-max)	*P*	*P* (pairwise)
MWA	1.302 (0.937–1.986) cm^3	1.532 (1.004–2.176) cm^3	6.056 (5.445–7.389) cm^3	0.003	0h–2h 1.00 0h–48h 0.004 2h–48h 0.024
MWA-cooling	1.445 (0.950–1.744) cm^3	1.699 (1.328–1.882) cm^3	1.981 (1.206–3.026) cm^3	0.045	0h–2h 0.838 0h–48h 0.039 2h–48h 0.479

Supplemental Table 2. The coagulation zone for RFA and RFA-cooling

	0h (n=6) Median (min-max)	2h (n=6) Median (min-max)	48h (n=6) Median (min-max)	*P*	*P* (pairwise)
RFA	1.102 (0.936–1.206) cm^3	1.202 (0.890–1.437) cm^3	4.187 (3.591–4.241) cm^3	0.003	0h–2h 1.00 0h–48h 0.004 2h–48h 0.026
RFA-cooling	0.849 (0.628–1.282) cm^3	1.033 (0.902–1.376) cm^3	1.133 (1.049–1.416) cm^3	0.030	0h–2h 0.479 0h–48h 0.024 2h–48h 0.641

Supplemental Table 3. The damage zone for MWA and MWA-cooling

	0h (n=6) Median (min-max)	2h (n=6) Median (min-max)	48h (n=6) Median (min-max)	*P*	*P* (pairwise)
MWA	1.070 (0.837–1.131) cm^3	4.818 (2.814–6.082) cm^3	6.056 (5.445–7.389) cm^3	0.001	0h–2h 0.092 0h–48h 0.001 2h–48h 0.390
MWA-cooling	1.495 (0.950–1.744) cm^3	1.645 (0.950–1.845) cm^3	2.068 (1.206–3.026) cm^3	0.037	0h–2h 1.00 0h–48h 0.048 2h–48h 0.145

Supplemental Table 4. The damaged zones for RFA and RFA-cooling

	0h (n=6) Median (min-max)	2h (n=6) Median (min-max)	48h (n=6) Median (min-max)	*P*	*P* (pairwise)
RFA	1.102 (0.936–1.206) cm^3	2.627 (1.761–3.732) cm^3	3.974 (3.465–4.308) cm^3	0.001	0h–2h 0.120 0h–48h <0.0001 2h–48h 0.251
RFA-cooling	0.890 (0.628–1,282) cm^3	0.994 (0.880–1.504) cm^3	1.133 (1.049–1.416) cm^3	0.045	0h–2h 0.641 0h–48h 0.039 2h–48h 0.641

Supplemental Table 5. The enlarged and transition zones in MWA and MWA-cooling

	MWA (n=6) Median (min-max)	MWA-cooling (n=6) Median (min-max)	*P*
Enlarged zone	4.700 (4.161–6.333) cm^3	0.963 (0.256–1.406) cm^3	0.002
Transition zone	4.486 (3.954–5.322) cm^3	0.642 (0.331–1.327) cm^3	0.002

Supplemental Table 6. The enlarged and transition zones in RFA and RFA-cooling

	RFA (n=6) Median (min-max)	RFA-cooling (n=6) Median (min-max)	*P*
Enlarged zone	3.041 (2.641–3.186) cm^3	0.496 (0.265–0.787) cm^3	0.002
Transition zone	2.881 (2.568–3.126) cm^3	0.433 (0.279–0.623) cm^3	0.002